Measurement of Minority-Carrier Diffusion Lengths Using Wedge-Shaped Semiconductor Photoelectrodes

Supplementary Information

Calculation of photocurrent
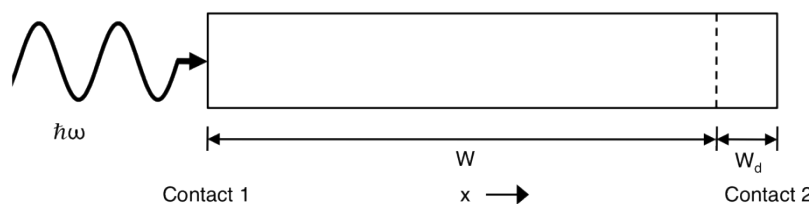
Fig. S1 Geometry for one-dimensional photocurrent calculation.

The device model assumes abrupt, full depletion of minority carriers (holes in our n-type semiconductor example system) at a depletion-width boundary at a distance W_d from a barrier-type contact; a back contact with an arbitrary recombination velocity; low-level injection with a bulk minority-carrier lifetime τ; and simple exponential light absorption, with each absorbed photon generating one electron-hole pair. The geometry used to set up the following model is shown in Fig. S1, where light is incident on the left side of a semiconductor slab at $x = 0$ through a transparent contact (Contact 1), and any light that is not absorbed escapes through Contact 2 on the right side of the diagram. Photogenerated charge carriers are lost either by bulk recombination or by collection at either boundary with a collection (or recombination) velocity s. The solution to the diffusion equation for excess minority holes is then:[10]

$$\Delta p(x) = A e^{-x/L_p} + B e^{x/L_p} + C e^{-\alpha x}, \tag{S1}$$

where the coefficients A, B, and C are given by

$$A = C\left(\frac{(S_2 - \alpha L_p)(1 - S_1)e^{-\alpha W} + (S_1 + \alpha L_p)(1 + S_2)e^{W/L_p}}{(1 - S_1)(1 - S_2)e^{-W/L_p} - (1 + S_1)(1 + S_2)e^{W/L_p}}\right),$$

$$B = C\left(\frac{(S_2 - \alpha L_p)(1 + S_1)e^{-\alpha W} + (S_1 + \alpha L_p)(1 - S_2)e^{-W/L_p}}{(1 - S_1)(1 - S_2)e^{-W/L_p} - (1 + S_1)(1 + S_2)e^{W/L_p}}\right),$$

$$C = \frac{(1-R)\,\Phi\,\tau\,\alpha}{1 - \alpha^2 L_p^2}$$

,

and the dimensionless boundary collection/recombination velocities are defined as $S = sL_p/D$, evaluated at the edges of the quasi-neutral region of width W. If the junction is on the right (front) side of the device, the assumed complete minority carrier sweep-out implies $S_2 \rightarrow \infty$. The photocurrent density resulting from full collection by drift in the depletion region, as well as partial diffusion collection by considering the continuity equation for carriers that diffuse to the depletion region boundary, is then:

$$\left| J_{photo}/e_c \right| = \int_{W}^{W+W_d} G(x)\,dx + D\frac{d\Delta p}{dx}\bigg|_{x=W}$$

, (S2)

where e_c is the charge on an electron. Equation S2 was implemented in Mathematica, and is plotted under various conditions in Fig. 1 in the main text.

Effect of porosity
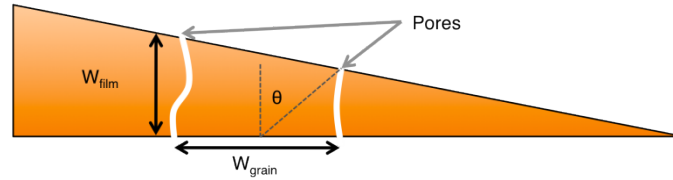
Fig. S2 Pore geometry considered allowing non-1-D minority-carrier collection.

Though porosity and nanostructuring can be a critical part of efficient electrode design for photoelectrochemical devices, any deviations from a dense, approximately planar film are potentially confounding issues for electrochemical diffusion-length measurements. Porosity in the film causes the 1-D approximation to break down because photogenerated carriers can be collected by electrolyte that has filled in any cracks or connected pores, and the effective film thickness for collection is therefore not the true film thickness. The simple 1-D model can be modified by replacing the film thickness with an effective film thickness, given by

$$W_{eff} = W_{film} \sin\left[\tan^{-1}\left(\frac{W_{grain}/2}{W_{film}}\right)\right],$$

(S3)

where the geometry under consideration is shown in Fig. S2. In the limit that $W_{grain} \to 0$, $W_{eff} \to 0$, while in the limit that $W_{grain} \to \infty$, $W_{eff} \to W_{film}$. Though this is a very crude correction to the 1-D model, it reasonably reproduces the behavior expected when 3-D collection is active. The photocurrent will then tend to become constant as a function of apparent film thickness, as shown in Fig. S3 where a correction has been made to the dotted-line base case without pores.
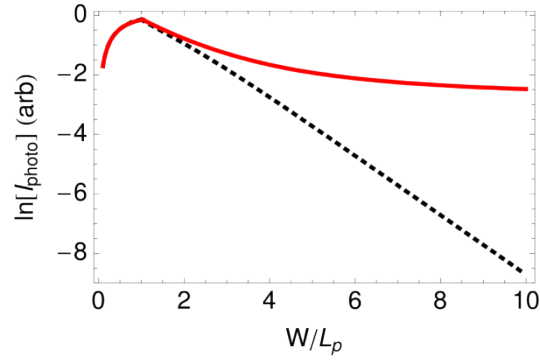
Fig. S3 Photocurrent behavior with pores. The black dotted line shows a base case with strongly absorbed light and high back-surface recombination without pores, and the red solid line is calculated with grains of width $W_{grain} = L_p/25$.

WO$_3$ Film Characterization

The tungsten oxide showed different film morphologies when films were grown at various substrate temperatures. XRD data for films deposited at different temperatures are shown in Fig. S4. All of the peaks could be matched to peaks ascribable to monoclinic WO$_3$, but the texture and grain size varied with growth temperature.
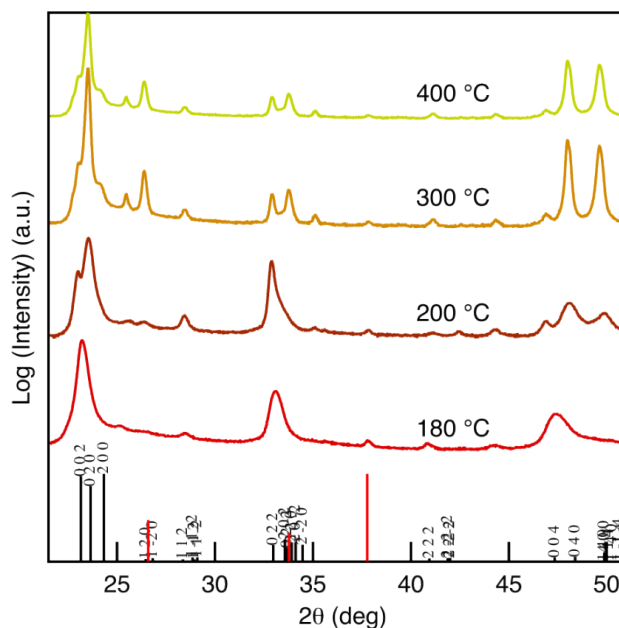
Fig. S4 X-ray diffraction data for WO_3 films deposited at various temperatures on $F:SnO_2$-coated glass. The substrate peaks are shown as unlabelled red lines at the bottom, whereas the labelled lines are peak positions for monoclinic WO_3.

The linear thickness profile of the Si wedge was simply measured by cleaving and examining the cross-sectional thickness of the sample, but determination of the thickness profile of the thin-film WO_3 sample required more in-depth examination. An example of the optical interference fringes used to determine the thickness profile is shown in Fig. S4. To characterize the gradient in thickness, the film that was simultaneously deposited on the Si wafer was imaged in an optical microscope. The Si wafer provided a clear view of the optical reflectance fringes so that a reflectance image with 500 nm illumination allowed determination of the film thickness profile. An ellipsometric measurement for a known thickness WO_3 film was used to determine that the index at 500 nm was 2.34, so each maximum in the interference fringe profile corresponded to a thickness increase of $\lambda/(2n)=107$ nm. The thickness profile was fitted to a sigmoidal function. Additionally, the films deposited on FTO were often cleaved at the thick side to image the cross-sectional film morphology in a scanning-electron microscope (SEM), and the maximum thickness could be verified or used to adjust the optical data. The films grown on FTO could also be used to image the thickness fringes, but the lower index contrast at the substrate as well as the underlying FTO roughness gave less interference contrast.
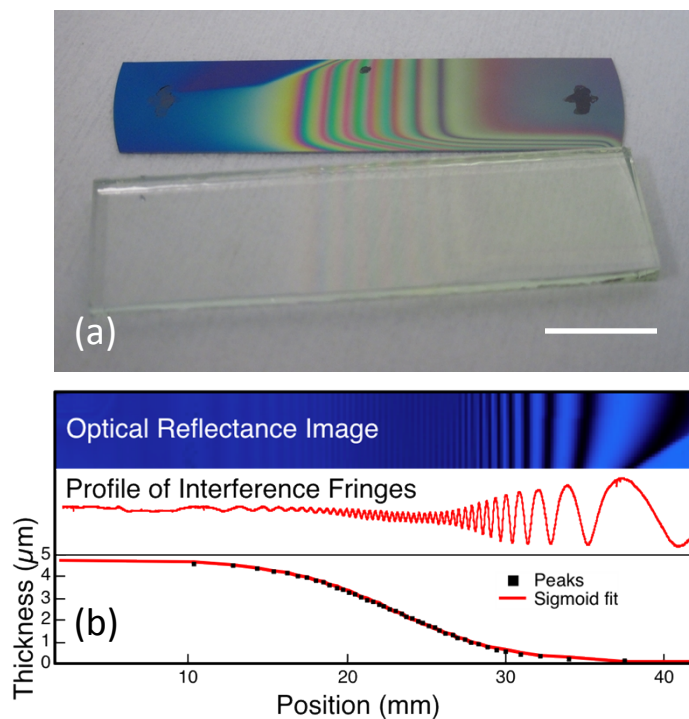
Fig. S5 (a) Image of WO$_3$ wedge film on Si (top) and on FTO (bottom). Scale bar is 10 mm. (b) Top: Image of reflectance of WO$_3$ wedge film on Si with illumination at 500-nm wavelength. Middle: Line profile of reflectance magnitude. Bottom: Thickness profile determined by positions of peak reflectance and known index.

An example of quiescent cyclic voltammetry under chopped illumination is shown in Fig. S6. The data were collected under chopped illumination so that the current both under illumination and in the dark was evident. The sweep was performed with the 1 mm focused illumination at an arbitrary point on the sample and under quiescent conditions, with some exposed FTO, so the absolute values were somewhat different than the standard case of fully filled front illumination on a well-sealed electrode. However, the general curve shape is as expected for WO$_3$, with an onset potential of 0.2-0.3 V vs. E(AgCl/Ag) (0.4-0.5 V relative to the hydrogen potential). The photocurrent never fully saturated in this voltage range but began to level off at voltages of ~0.8-0.9 V vs. $E_{Ag/AgCl}$. For reference, the oxygen-evolution potential in this cell is at 1.03 V vs. E(AgCl/Ag).
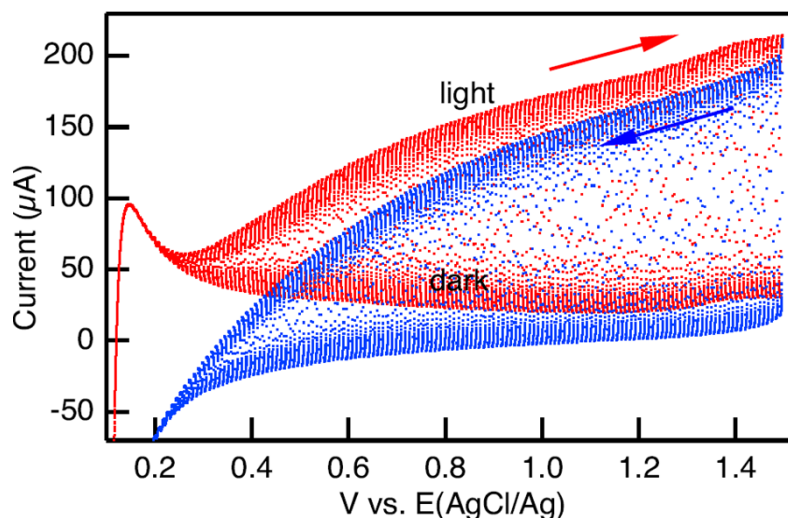
Fig. S6 Cyclic voltammetry sweep of WO$_3$ film under chopped 365-nm illumination.

Insulation of pores in porous WO$_3$

After sputtering, the tungsten oxide was often too porous to obtain robust electrochemical data. To insulate the electrochemically active pores or grain sidewalls, the sample surface was coated with a 10 nm layer thick of aluminum oxide that was deposited by atomic layer deposition (ALD - Cambridge Nanotechnology). A 20 sec diffusion time in exposure mode was used to allow the precursor to fully diffuse inside the pores. The ALD-treated samples showed no electrochemical activity or photocurrent, verifying that the alumina was largely conformal and insulating, as desired. To expose the top surface, the samples were mounted on the tripod polisher, and were carefully levelled by use of a flat glass plate and by minimization of the number of Newton's rings visible between the plate and the sample. Gentle polishing was then performed using 50 nm colloidal diamond slurry (Buehler MetaDi Supreme 0.05um) on a porous polyurethane pad (Eminess Politex Reg) for 10-30 min on a polishing wheel rotated at ~50 rpm. The best results and uniformity were obtained when the sample was rotated once or twice during polishing. For short polishing times, only the tops of the largest and highest-protruding grains were polished, as evidenced by the low SEM contrast and flat profile in an atomic-force microscope (AFM) scan. With somewhat longer polishing, most of the top grains were polished smooth, as evidenced by SEM images. As the sample was polished even further, the surface became extremely flat and was difficult to image in the SEM. One sample was also gently sputtered using the RF substrate bias in the AJA sputtering system. This process revealed the pores that had been insulated by aluminum oxide, because the tungsten oxide was more readily sputtered, leaving behind the aluminum oxide that had coated the sidewalls as protrusions.

Large illumination spot scanned along a wedge with non-linear thickness variation

In the diffusion-length measurement analysis, a point spot illumination scanned over a film with a thickness gradient was assumed. This procedure produced a photocurrent that exhibited an exponential decay with thickness, $J(w) = J_0\, e^{-w/L}$, where w is the thickness at the measurement spot and L is the minority-carrier diffusion length. The experimental system however had a finite spot size, which produced a photocurrent value averaged over the illumination area with a gradient thickness. To evaluate the impact of the beam size on the diffusion length measurement, we assume a large beam spot incident on a wedge having a non-linear thickness variation (Fig. S7).
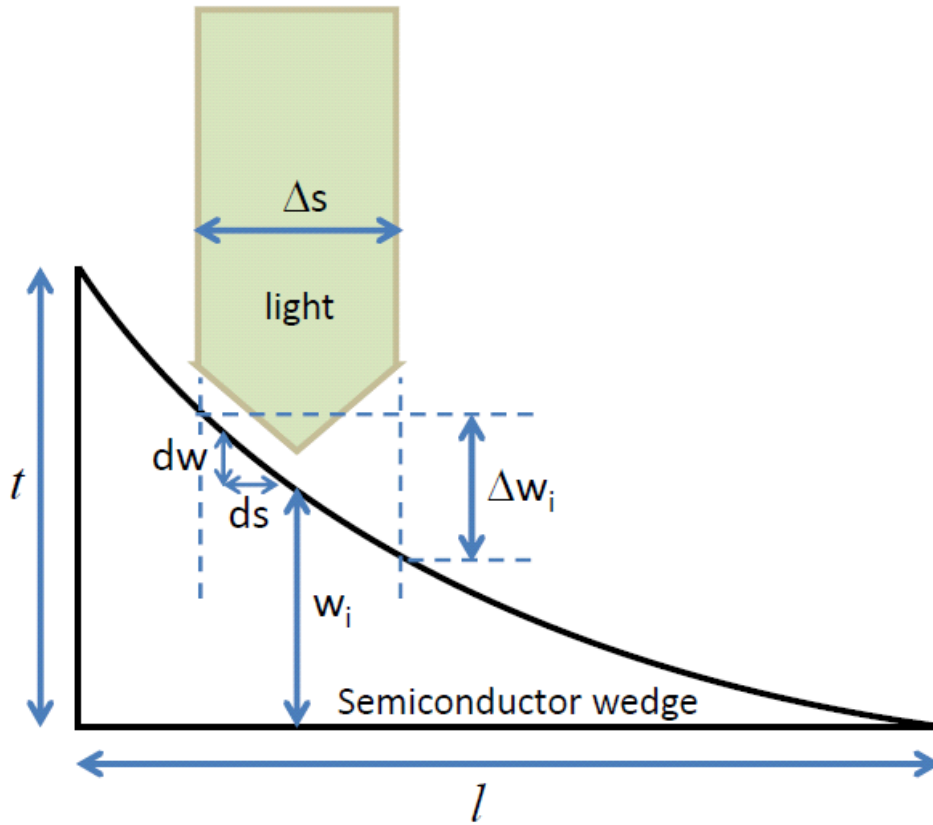
Fig. S7 Schematic of a wedge with non-linear thickness variation illuminated by a large beam.

The average photocurrent at any point, i, can be calculated by integrating the photocurrent over the illuminated area:

$$\bar{J}_i = \frac{1}{\Delta s}\int_i J(w(s))\, ds \approx \frac{1}{\Delta w_i}\int_i J(w)\, dw$$

Here we assume the spot size, Δs, is small compared to wedge length, l, $\Delta s \ll l$. The thickness gradient in each segment Δs is therefore assumed to be linear, i.e. $\dfrac{dw}{ds} = const$.

$$\bar{J}_i = J_0 \frac{1}{\Delta w_i} \int_{w_i - \Delta w_i/2}^{w_i + \Delta w_i/2} e^{-w/L}\, dw$$

$$\bar{J}_i = J_0 e^{-w_i/L} \left\{ \frac{L}{\Delta w_i} \left(e^{\Delta w_i/2L} - e^{-\Delta w_i/2L} \right) \right\}$$

(S4)

$$\bar{J}_i = J_0 e^{-w_i/L} \frac{L}{\Delta w_i} \left(1 + \frac{\Delta w_i}{2L} + \left(\frac{\Delta w_i}{2L}\right)^2 \frac{1}{2} + \left(\frac{\Delta w_i}{2L}\right)^3 \frac{1}{6} + \cdots - 1 + \frac{\Delta w_i}{2L} - \left(\frac{\Delta w_i}{2L}\right)^2 \frac{1}{2} + \left(\frac{\Delta w_i}{2L}\right)^3 \frac{1}{6} - \cdots \right)$$

$$\bar{J}_i = J_0 e^{-w_i/L} \left(1 + \left(\frac{\Delta w_i}{L}\right)^2 \frac{1}{24} + \left(\frac{\Delta w_i}{L}\right)^4 \frac{1}{1920} + \cdots \right)$$

for $\Delta w_i < L$:

$$\bar{J}_i \approx J_0 e^{-w_i/L}$$

The photocurrent is thus simply given by an exponential decay, provided that the thickness gradient is small, i.e. $\Delta w_i < L$.

The value of $\dfrac{\Delta w_i}{L}$ can be approximately given by $\dfrac{\Delta w_i}{L} \sim \dfrac{\Delta s\, t}{l\, L}$, where $\dfrac{t}{L}$ is the ratio of the film thickness to the minority-carrier diffusion length. In our experiments, an illumination spot size of $\Delta s \approx 1\,mm$ was scanned over a wedge length of $l = 25\,mm$. Additionally, the film thickness was 2-3 times larger than the minority-carrier diffusion length for each sample. Therefore $\dfrac{\Delta w_i}{L}$ values were on the order of ~0.1 in the experiments.

Note that the requirement for small thickness gradient is less stringent when the wedge has a nearly uniform gradient. When the thickness gradient is constant, the photocurrent decay is given by the expression S4, which has the same exponential form but with an additional, constant, prefactor:

$$\bar{J}_i = J_0 e^{-w_i/L} \left\{ \frac{L}{\Delta w_i} \left(e^{\Delta w_i/2L} - e^{-\Delta w_i/2L} \right) \right\}$$

$$\bar{J}_i = J_0' e^{-w_i/L}$$

Diffusion length measurement on a wedge with non-uniform thickness variation

A non-uniform thickness can be a critical limitation in the determination of accurate minority-carrier diffusion lengths by the method developed herein. To evaluate the impact of non-uniform thickness variation, we assume that the films has a random thickness fluctuation characterized by a Gaussian

distribution, as well as a large number of fluctuations within the illumination area. Assuming a thickness fluctuation with a standard deviation of σ, the average photocurrent over the illumination spot is given by:

$$\bar{J}_i = \int_{-\infty}^{\infty} F(w) \, J_0 \, e^{-w/L} dw = \frac{1}{\sigma\sqrt{2\pi}} J_0 \int_{-\infty}^{\infty} e^{-\frac{(w-w_0)^2}{2\sigma^2}} e^{-\frac{w}{L}} dw$$

where w is a random thickness value in the distribution, w_0 is the average thickness and L is the minority-carrier diffusion length.

$$\bar{J}_i = \frac{1}{\sigma\sqrt{2\pi}} J_0 \, e^{-\frac{w_0}{L}} \int_{-\infty}^{\infty} e^{-\frac{u^2}{2\sigma^2}} e^{-\frac{u}{L}} du$$

$$\bar{J}_i = e^{\frac{\sigma^2}{2L^2}} J_0 \, e^{-\frac{w_0}{L}} \qquad\qquad (S5)$$

$$\bar{J}_i = J_0{'} \, e^{-\frac{w_0}{L}}$$

The final expression indicates that that random fluctuations on the sample thickness will add a constant prefactor to the photocurrent expression, and thus will increase the absolute value of the measured photocurrent values while the exponential decay rate of the photocurrent with thickness remains the same. Furthermore, this prefactor can be ignored if the standard deviation is small compared to the minority-carrier diffusion length, *i.e.*, $\sigma \ll L$. Note that in this derivation, we assumed the standard deviation remained the same along the thickness gradient. If thickness fluctuations were induced by film growth etc. then careful characterization of thickness variation would be required, especially if the fluctuations were comparable to the minority-carrier diffusion length. The samples used in our experiments were polished on top and the fluctuation in the thickness (~ 5 - 10 nm) was mainly caused by the substrate roughness (FTO). Hence the assumption of a constant standard deviation along the surface is justified for this experimental arrangement.